nature structural & molecular biology

Hypermutation by intersegmental transfer of APOBEC3G cytidine deaminase

Roni Nowarski, Elena Britan-Rosich, Tamar Shiloach & Moshe Kotler

Deamination of cytidine residues in single-stranded DNA (ssDNA) is an important mechanism by which apolipoprotein B mRNA-editing, catalytic polypeptide-like (APOBEC) enzymes restrict endogenous and exogenous viruses. The dynamic process underlying APOBEC-induced hypermutation is not fully understood. Here we show that enzymatically active APOBEC3G can be detected in wild-type Vif(+) HIV-1 virions, albeit at low levels. *In vitro* studies showed that single enzyme-DNA encounters result in distributive deamination of adjacent cytidines. Nonlinear translocation of APOBEC3G, however, directed scattered deamination of numerous targets along the DNA. Increased ssDNA concentrations abolished enzyme processivity in the case of short, but not long, DNA substrates, emphasizing the key role of rapid intersegmental transfer in targeting the deaminase. Our data support a model by which APOBEC3G intersegmental transfer via monomeric binding to two ssDNA segments results in dispersed hypermutation of viral genomes.

DNA binding proteins can locate specific sequences at a rate exceeding the theoretical limit imposed by the diffusion control of particles in aqueous solution[1]. This phenomenon was termed 'facilitated diffusion', based on the principle that specific target-site location is facilitated by nonspecific electrostatic binding of proteins to DNA[2–5]. Translocation of proteins on DNA was suggested to occur either in a positionally correlated fashion—that is, by one-dimensional (linear) sliding or microscopic jumping—or in an uncorrelated fashion—by three-dimensional macroscopic jumping or intersegmental transfer[2–5] (**Fig. 1**). Intersegmental transfer requires a protein unit (monomeric or multimeric) containing two DNA binding sites for binding two DNA segments simultaneously, thereby maintaining intimate contact with DNA; in contrast, during macroscopic jumping the protein moves through bulk solution. Although facilitated diffusion was traditionally assigned to a linear sliding motion of proteins on DNA, it was shown that target location by the EcoRV endonuclease is mediated by a combination of sliding and successive three-dimensional dissociations and reassociations to DNA[6]. Whereas evidence for three-dimensional transfer between DNA binding sites via free solution is available also for other DNA binding proteins[7–10], intersegmental transfer has not yet been demonstrated as a major path in protein targeting. Attractively, formation of a ternary protein-DNA intermediate that would suggest such a mechanism was reported for the *Escherichia coli* ssDNA binding proteins RecA[11] and Ssb[12]. Structures of proteins bound to double-stranded DNA motifs suggested a role for DNA looping in DNA cleavage[13,14], repression[15] and recombination[16].

Apolipoprotein B mRNA-editing, enzyme-catalytic polypeptide-like 3G (referred to here as A3G) is a member of a cellular cytidine deaminase family encoded within a cluster of seven APOBEC3 (A3) genes on chromosome 22, designated A3A, B, C, DE, F, G and H[17]. A3 proteins are innate antiviral restriction factors, acting as potent editors of foreign ssDNA[18–20]. Other family members (reviewed in ref. 18) include APOBEC1, an mRNA editor in gastrointestinal cells involved in the metabolism of apolipoprotein B, activation-induced deaminase (AID), a lymphoid-specific DNA deaminase involved in B cell maturation and antibody diversification, and APOBEC2, whose expression is restricted to heart and skeletal muscle but whose function is still unknown. All APOBEC proteins share a zinc-coordinating cytosine/cytidine deaminase domain defined by a conserved HXE-$X_{23–28}$-CP$X_{2–4}$C motif, in which the glutamic acid residue promotes hydrolysis and catalysis[21,22]. A3B, A3F and A3G contain a duplication of this domain, wherein the N-terminal domain is probably dominant in RNA binding and the C-terminal domain in deamination[23,24]. A3G is involved in the restriction of human immunodeficiency virus[25–30] (HIV-1) and hepatitis B virus[31–34] infection, as well as inhibition of endogenous retrotransposition[35–38]. During infection with HIV-1$^{vif(-)}$, in which the viral genome lacks the gene for the virion infectivity factor (Vif), A3G is incorporated into assembled virions, leading to hypermutation and inactivation of the nascent viral cDNA generated by reverse transcription in target cells[27,28,30,39]. During natural HIV-1 infection, Vif prevents lethal editing of the viral genome by targeting cellular A3G to proteasomal degradation via formation of an E3-ligase complex[25,29,40–42], by inhibiting A3G translation[41] and by preventing A3G virion incorporation[43].

Whereas these viral defense strategies used by Vif certainly hinder A3G packaging into virions, here we report that enzymatically active A3G is incorporated into wild-type HIV-1 virions produced in H9

Department of Pathology and the Lautenberg Center for General and Tumor Immunology, the Hebrew University-Hadassah Medical School, Jerusalem 91120, Israel. Correspondence should be addressed to M.K. (mkotler@cc.huji.ac.il).

Received 7 May; accepted 2 September; published online 28 September 2008; doi:10.1038/nsmb.1495

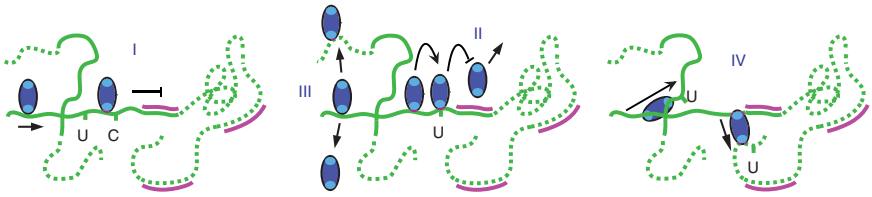

Figure 1 Models for A3G translocation during retroviral reverse transcription. Intermittent cleavage by viral RNase H leaves RNA fragments (purple) annealed to the viral cDNA (green). Monomeric A3G (ovals) translocation on ssDNA by sliding (I), microscopic or macroscopic jumping (II and III, respectively) and intersegmental transfer (IV) is illustrated. In sliding, A3G proceeds linearly along DNA, deaminating consequent targets until it reaches an RNA-DNA duplex. Similarly, microscopic jumping directs correlated motion via local dissociation-reassociation steps. Macroscopic jumping involves A3G motion through solution, overcoming local physical barriers while risking disengagement from the DNA. Intersegmental transfer promotes dispersed deamination while maintaining contact with DNA.

cells. To study the mechanism of A3G DNA editing, we purified A3G from HEK-293T cells and measured its local and global activity on short and long ssDNA substrates. Our results show that A3G target location is based on positionally uncorrelated nonlinear translocation on ssDNA. Uniquely, although A3G acted distributively on adjacent cytidines, it performed deamination of numerous targets separated by various distances. A3G resided mostly in multimers, but bound DNA as a monomer. A notable feature of monomeric A3G was its ability to bind two DNA fragments simultaneously. Thus, we propose that A3G-induced hypermutation of viral genomes is mediated by intersegmental transfer of A3G monomers on ssDNA.

RESULTS

Active A3G is incorporated into wild-type HIV-1 virions

A3G packaging into HIV-1 virions is counteracted by the viral Vif protein in virus-producing cells[25,29,42,43]. To determine whether A3G evades Vif activity in HIV-1 natural target cells, we developed a highly sensitive assay for detection of cytidine deamination (**Fig. 2a** and **Supplementary Fig. 1** online). The deamination assay is based on differential cleavage by specific restriction endonucleases following PCR amplification of A3G reaction products, and it allows detection of the mutational bias resulting from cytidine deamination in a reaction containing under 10^{-17} mol A3G. Purified wild-type virions produced in H9 cells expressing A3G endogenously contained deaminase activity (**Fig. 2b**). No deamination was associated with virions produced in A3G-nonexpressing SupT1 cells (not shown) or mock-infected H9 cells (**Fig. 2b**), indicating that deamination was due to active A3G incorporated into HIV-1 virions in virus-producing cells. RNase treatment increased the deaminase activity associated with the wild-type and *vif*$^{(-)}$ viruses, suggesting association of A3G with RNA[44]. Deaminase activity associated with *vif*$^{(-)}$ virions was 12-fold to 20-fold higher than in wild-type virions when adjusted for the p24 content used in the assay. Although A3G was detected in a *vif*$^{(-)}$ virus produced in H9 cells by western blot analysis, A3G levels associated with the equivalent p24 content (18 ng) of wild-type virus were below the detection threshold of the assay (**Fig. 2c**), consistent with published data[25,29,41]. Evaluating (i) deamination levels of virus-associated A3G relative to purified A3G, (ii) purified A3G–specific activity and (iii) the amount of p24 used in the deamination assay, we calculated that the ratio of active A3G to HIV-1 Gag polyprotein precursor ($Pr55^{Gag}$) is 1:6,520 in the wild-type virus, and 1:551 in the *vif*$^{(-)}$ virus. It is estimated that each HIV-1 virion contains 2,000 or 5,000 Gag molecules[45,46]; therefore, on average, there are approximately 0.3–0.8 active A3G molecules for each wild-type virion, and 4–9 active A3G molecules for each *vif*$^{(-)}$ virion. Thus, a naturally occurring wild-type viral population may contain a potentially lethal cargo of A3G. Whether virion-associated A3G has any negative or positive effects on HIV-1 replication remains to be established.

Correlation to facilitated diffusion

To study the basis for A3G-induced hypermutation, we prepared a highly active recombinant enzyme by expressing a myc-His_6-tagged human A3G protein in HEK-293T cells[40]. A3G was efficiently purified by Ni^{2+}-affinity chromatography (>85%) only after treatment of cell lysates with RNase A and 0.8 M NaCl, which are required to dissociate A3G from high molecular mass (HMM) complexes formed in these cells[38,47] (**Fig. 3a**). As facilitated-diffusion processes are based on electrostatic protein-DNA interactions, we measured initial deamination rates as a function of the solution ionic strength. Deamination of the CCC-containing 80-nt substrate S_{Eco} (**Supplementary Table 1** online) was inversely proportional to NaCl (**Fig. 3b**) or NH_4Cl (not shown) concentration, suggesting that strong electrostatic interaction

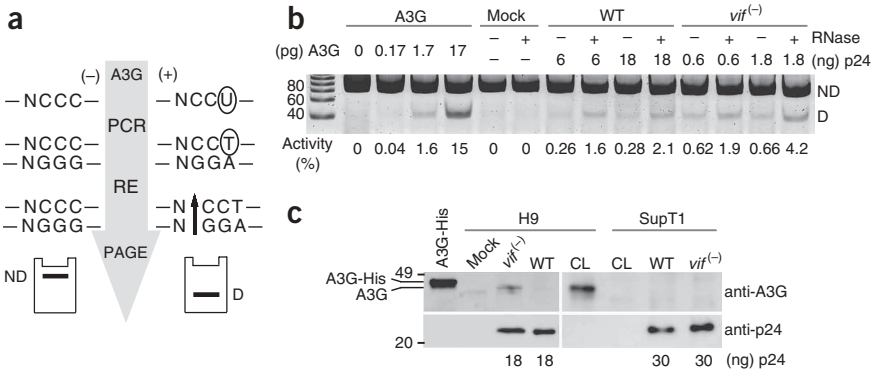

Figure 2 Enzymatically active A3G is incorporated into HIV-1 virions. (**a**) Scheme of the deamination assay. Incubation of a single-stranded deoxyoligonucleotide with A3G results in deamination and C→U conversion within the A3G target motif, generating a restriction-enzyme recognition sequence following PCR. D, deaminated; ND, not deaminated; RE, restriction enzyme. (**b**) Deaminase activity associated with wild-type (WT) and Δ*vif* (*vif*$^{(-)}$) HIV-1 produced in H9 cells. Deaminase activity in concentrated culture medium of mock-, *vif*$^{(-)}$- or wild-type HIV-1_{HXBII}-infected H9 cells was measured by incubation with S_{Eco} in the presence (+) or absence (–) of RNase A. Reactions were performed with the indicated amounts of purified A3G to determine the amount of active A3G in virions. The p24 content in virus-containing samples, deaminase-activity values and specific oligonucleotide sizes are indicated. (**c**) Western blot analysis of A3G in wild-type and *vif*$^{(-)}$ HIV-1 virions produced in H9 or SupT1 cells (above). The rabbit antiserum used recognizes the A3G C terminus. The HIV-1 CA protein, which used as a loading control, was detected by blotting the same membrane with mouse p24 antiserum (below). The p24 content in virus-containing samples (as determined by the HIV-1 p24 Antigen Capture Assay kit) and specific protein sizes (in kDa) are indicated. CL, cell lysate.

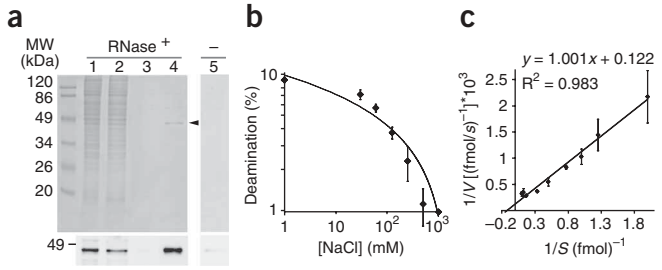

Figure 3 Correlation to facilitated diffusion. (**a**) Purification of A3G-myc-His_6 from HEK293T cells with (left) or without (right) pretreatment with RNase A. Protein samples were resolved by SDS-PAGE and stained with Imperial protein stain (above) or subjected to western blotting with an anti-myc antibody (below). Lane 1, cell lysates; lane 2, flow through; lane 3, wash; lanes 4 and 5, elution. The protein band corresponding to A3G is marked with an arrowhead. (**b**,**c**) Salt-dependence curve (**b**) and Lineweaver-Burk curve (**c**). Initial deamination rates were measured using 10 fmol S_{Eco} at E/S = 1:100 (**b**) or 1–300 fmol S_{Eco} at E/S = 1:10–1:3,000 (**c**; Methods) after 8 min incubation. Results are the average of at least four independent experiments; error bars indicate s.d.

between A3G and DNA is required for efficient catalysis. To directly assess the involvement of facilitated diffusion in A3G translocation, we measured the K_m of S_{Eco}, and then used the k_{cat}/K_m ratio as an approximation of the second-order rate constant for cytidine deamination by A3G[48]. The apparent K_m and k_{cat} values derived from the reciprocal $1/V_0$ versus $1/S$ plot (**Fig. 3c**) are 0.82 (± 0.06) nM and 0.163 (± 0.04) s^{-1}, respectively, giving a specificity constant of 2.0×10^8 M^{-1} s^{-1}. Such a high rate for the overall enzymatic process implies that target location involves some form of facilitated diffusion so that it will not be rate limiting[4].

A3G acts distributively on adjacent cytidines

Sequences of viral DNA produced on a $A3G^{(+)}/vif^{(-)}$ background, in the case of HIV-1 (refs. 27,28,30,39), murine leukemia virus[26] or hepatitis B virus[31,33], revealed that deamination occurs preferentially at C_3 of the 5′$C_1C_2C_3$ 3′ motif. However, a single polycytidine site may contain several potential targets, as deamination often occurs at adjacent cytidines (in the context of two, three or more cytidines) and, to a lesser extent, exclusively at cytidines other than C_3. To determine the deamination kinetics within a single target site, we used ss-deoxyoligonucleotides (80 nucleotides (nt)) containing one central CCC site, designed to indicate deamination of single or multiple cytidines within the target site (**Supplementary Table 1**). The distribution of deamination within the target site was assessed as a function of A3G concentration using S_{Eco} in conjunction with HaeIII or Eco147I, indicating the deamination levels at C_1 or C_2 ($C_{1/2}$), or exclusively at C_3 (C_3^{Ex}), respectively (**Fig. 4a**). Total deamination ($C_{1/2/3}$) was measured with the substrate–restriction enzyme combination S_{Apa}/ApaI, which was also used as an internal assay control assuming that this value should equal the sum of $C_{1/2}$ and C_3^{Ex} deamination levels. Whereas deamination levels at both C_3 and $C_{1/2}$ increased proportionally with enzyme concentration, deamination at C_3 was the most prominent and accounted for the majority of deaminated substrate at all assayed concentrations. Deamination at $C_{1/2}$, on the other hand, was highly dependent on enzyme concentration, accounting for only 1% of the total deaminated substrate at 10 pM A3G (enzyme:substrate ratio (E/S) = 1:100) and reaching 40% at 0.5 nM A3G (E/S = 1:2). The low levels of $C_{1/2}$ deamination at low A3G concentration were further corroborated by measuring the initial reaction rates at 10 pM A3G and excess of S_{Eco} (E/S = 1:100, **Fig. 4b**). Deamination occurred almost exclusively at C_3, and only marginally at $C_{1/2}$ after 4 min incubation, in spite of the intermolecular cycling required to deaminate ~8 mol of substrate over 1 mol enzyme (0.8 fmol product per 0.1 fmol enzyme).

To verify that deamination at $C_{1/2}$ is feasible on a C_3-deaminated substrate, we used the CCU-containing 80-nt substrate S_{CCU} and compared the rate of deamination at $C_{1/2}$ with S_{Eco} or S_{CCT} (**Supplementary Fig. 2a** online). Whereas deamination rates were similar for S_{CCU} and S_{CCT}, deamination of $C_{1/2}$ in S_{Eco} was slower, increasing with time as most of the substrate is deaminated at C_3 to produce a CCU sequence. On the basis of the higher rate of C_3 deamination and the decline of C_3^{Ex} deamination at high enzyme concentrations (**Fig. 4a**), it seemed possible that deamination at $C_{1/2}$ was dependent on deamination at C_3. We therefore measured the deamination kinetics within a CCC target site at 0.5 nM A3G using S_{Psi}/PsiI (E/S = 1:2) to indicate deamination at C_{2+3} (C_2 and C_3, **Supplementary Fig. 2b**).

We also used S_{Psi}/AseI to indicate deamination at C_1; however, no deamination was observed above background levels. We will therefore treat $C_{1/2}$ as C_2 from here on. Subtraction of the deamination levels at C_{2+3} from C_2 points out that, at early reaction times, deamination at C_2^{Ex} occurred at a higher rate (approximately two-fold) than at C_{2+3},

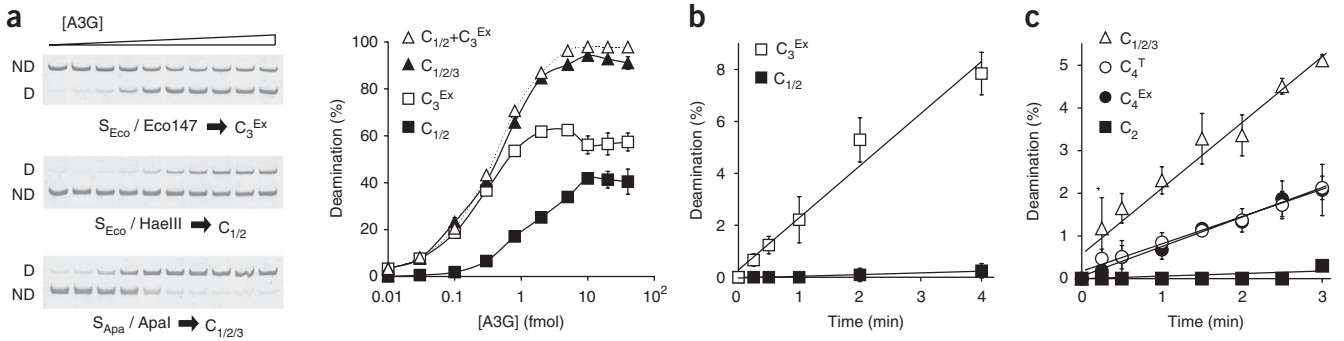

Figure 4 A3G acts distributively on adjacent cytidines. (**a**) Deamination at C_3^{Ex}, $C_{1/2}$ and $C_{1/2/3}$ was measured using S_{Eco} or S_{Apa} after 8 min incubation with increasing amounts of A3G. Left, PAGE images of PCR products cleaved with the indicated restriction endonucleases. Note that in the case of S_{Apa}/ApaI and S_{Eco}/HaeIII, deamination was assessed by the amount of noncleaved substrate. S_{Eco}/Eco147I indicates deamination at C_3^{Ex} because additional deamination at the same site will result in the loss of the Eco147I recognition sequence. (**b**) Initial deamination rates (E/S = 1:100) at C_3^{Ex} and $C_{1/2}$ were measured using S_{Eco}. (**c**) Initial deamination rates (E/S = 1:100) at C_4^{Ex} $C_{1/2/3}$ and C_2 were measured using the S_{Pas} CCCC-containing substrate, and at C_4^T using S_{Mse}. See text and **Supplementary Table 1** for specific usage of restriction enzymes and abbreviations. D, deamination; ND, not detected. Results are the average of at least four independent experiments; error bars indicate s.d.

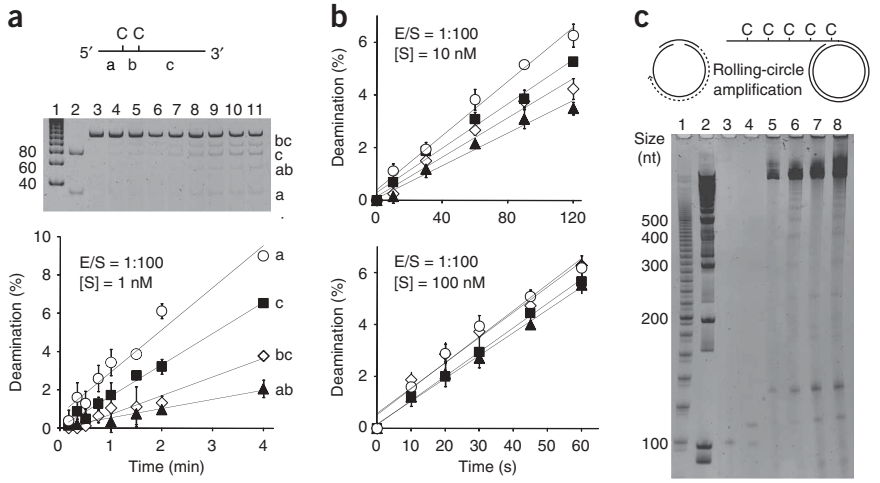

Figure 5 Segmental and molecular transfer of A3G. (**a**) Initial deamination rates were measured at 1 nM of the double CCC substrate S_{130} (E/S = 1:100). Deamination rates at each or both sites (3′/5′) were assessed according to the formation of the specific size of the restriction products. Lane 1, 20-nt marker. Lane 2, HaeIII restriction products indicated total cleavage of the substrate. Note that SYBR-gold staining is both size and sequence dependent. Hence, staining intensities were three times higher for the c over the a fragments (lane 2) and 2.2 times higher for the ab over a fragments (not shown). Lanes 3–11, reactions times: 0 s, 10 s, 20 s, 30 s, 45 s and 1 min, 1.5 min, 2 min and 4 min, respectively. (**b**) Initial deamination rates were measured as in **a** in the presence of 10 nM (above) or 100 nM (below) S_{130} (E/S = 1:100). (**c**) *In vitro* rolling-circle amplification was used to generate 5–10 kb substrates containing CCC targets in 100-nt intervals. Reactions were performed without or with A3G at 50 nM substrate (E/S = 1:50, lanes 5 and 6, respectively), or at 100 nM substrate (E/S = 1:100, lanes 7 and 8, respectively). Lanes 1 and 2, 20-nt and 100-nt markers, respectively. Lanes 3 and 4, the 100-nt template, before and after ligation, respectively.

suggesting that deamination at C_2 occurs independently of deamination at C_3. At later times, deamination levels of C_{2+3} equal those of C_2, as most of the substrate is deaminated at C_3. The increased deamination of C_{2+3} is reflected also in the reduction in C_3^{Ex} deamination levels after 10 min incubation (**Supplementary Fig. 2b**). A3G preference for deamination at C_3 might be due to 3′→5′ directionality[49,50]. To test whether the C_3 3′-terminal position accounts for higher susceptibility to deamination, we measured initial deamination rates using S_{Pas}/PasI, ApaI or HaeIII to determine deamination at C_4^{Ex}, $C_{1/2/3}$ or C_2, respectively, and S_{Mse}/MseI to indicate C_4^T (total, **Fig. 4c**). Although substantial, deamination at C_4 was almost three times less efficient than at C_3, accounting for only 27% of total deamination. Notably, deamination rates at C_4^{Ex} and C_4^T were similar, indicating that deamination at C_4 was exclusive with no additional deamination at adjacent cytidines. Our results suggest that, locally, A3G deaminates a single cytidine per DNA binding event. This distributive mode of action does not support local sliding motion following catalysis.

Segmental and molecular transfer

Processive deamination of C_3 in separated CCC motifs was reported previously[49] but had also been inferred from the existence of heavily mutated viral DNA sequences after a single round of replication in the presence of A3G[26–28,30,39]. Enzyme translocation on DNA could be examined in view of the processive catalysis of two or more targets on the same substrate molecule[6]. We therefore assessed A3G activity using a 130-nt substrate containing two CCC sites located at the 5′ end (S_{130}), designed to increase the chance of random binding 3′ to the target sites. Initial rates of deamination at each or both sites were determined according to levels of restriction-reaction products of the correct size (**Fig. 5a**). Measurements of C_3 deamination under standard conditions showed processive catalysis by A3G with preference to the 5′ site, as evidenced by the higher rate of DNA fragment formation $(V_a+V_c)/(V_{ab}+V_{bc})$, and of V_a/V_c, in agreement with previous findings[49]. Assuming nonspecific binding and 3′→5′ directionality, the theoretical rate ratio V_{bc}/V_c is 0.28, according to b/c length ratio. However, the experimental rate ratio V_{bc}/V_c was 0.60, suggesting that singular deamination events at the 5′ site, which lead to formation of the bc fragment, occurred two-fold more rapidly than expected. This could not be attributed to a sliding motion from either direction; alternatively, nonlinear translocation that would direct an enzyme bound to the c segment over the 3′ site to the 5′ site could be envisaged. In this case, increasing the substrate concentration while maintaining E/S = 1:100 should result in enhanced intermolecular translocations, consequently reducing enzyme processivity. Indeed, initial deamination rates at 10 nM substrate showed reduced enzyme processivity, as seen by a lower ratio for $(V_a+V_c)/(V_{ab}+V_{bc})$ (**Fig. 5b**, above). Further increasing substrate concentration to 100 nM resulted in abrogation of A3G processivity, as seen by similar rates for V_a and V_{bc} and for V_c and V_{ab} (**Fig. 5b**, below). These results argue against sliding or microscopic jumping as major mechanisms involved in A3G translocation, as in those cases enzyme processivity would not dramatically decrease with increased DNA concentrations. Nonlinear translocation within the oligonucleotide substrate was validated using a 160-nt substrate (S_{160}) containing three 5′-located CCC sites (**Supplementary Fig. 3** online). The formation of the 32-nt bc fragment under standard conditions indicates that a single enzyme deaminated C_3 at the 3′ site and at the 5′ site, but not at the middle site.

Natural DNA targets of A3G, as in the case of HIV-1, might be several kilobases long. Assessment of A3G activity on long DNA substrates could therefore better reflect enzyme activity *in vivo*. We used *in vitro* rolling-circle amplification to produce ssDNA templates of 5–10 kb, each containing a CCC site at 100-nt intervals (**Fig. 5c**). Following incubation with A3G at 50–100 nM substrate (E/S = 1:50–100), DNA was treated with uracil-DNA glycosylase (UDG) to form abasic sites at converted deoxycytidines, which were further cleaved by NaOH treatment. Complete cleavage of DNA was verified by using S_{CCU} at a molar excess of targets (not shown). We expected that positionally correlated linear (sliding) or nonlinear (microscopic jumping) translocation would direct consecutive deamination events, predominantly leading to the formation of a 100-nt product, whereas positionally uncorrelated nonlinear translocation would produce products longer than 100 nt. Although there was no indication for the formation of the 100-nt product, we observed the formation of products of 200 nt to >1,000 nt long (**Fig. 5c**). Product formation was due to A3G activity, and was not a consequence of nonspecific factors affecting DNA stability, because, in the absence of A3G, in the absence of UDG, or in the presence of an A3G RNase$^{(-)}$ purification sample (**Fig. 3a**), no DNA cleavage products were detected (**Fig. 5c** and data not shown). Considering that only a small fraction of the

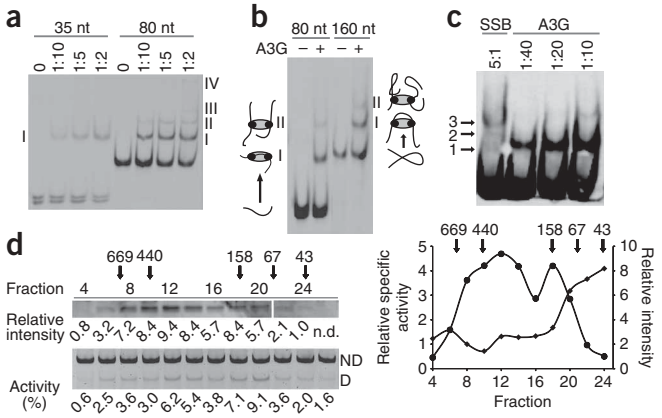

Figure 6 DNA tethering by monomeric A3G. (**a**) Binding of A3G to S_{35} and S_{Eco} shown by EMSA following 8 min incubation. Ratios of E/S used are indicated above. Roman numbers (I–IV) indicate shifted DNA bands. (**b**) EMSA showing A3G binding to S_{Eco} or S_{160} following 8 min incubation at E/S = 1:10. Cartoon ovals represent A3G bound to one or two DNA segments. (**c**) EMSA using T_4 SSB and A3G following 15 min incubation at the indicated E/S ratios. Arrows mark DNA bands shifted by SSB. (**d**) Western blot analysis of purified A3G following FPLC size exclusion (above, and right curve, ●), and activity of individual fractions on S_{Eco} (below). The relative specific activity (RSA) of individual fractions (right curve, ♦) was calculated by assigning fraction 24 a relative intensity value of 1, and using the following equation: RSA = (activity/relative intensity) × 200. D, deamination; ND, not detected. Protein markers (kD) used for molecular weight estimations are indicated with arrows.

substrate was deaminated (<15%), and assuming no more than one enzyme per DNA molecule, the reaction products represent deamination via intra- and intersegmental translocation (Methods). This might be anticipated by the fact that long DNA segments in solution form microdomains[2–4]. Accordingly, the DNA concentration used in the assay (50–100 nM) is not expected to dramatically reduce enzyme processivity via intermolecular transfer, as was observed in the case of the oligonucleotide substrate (**Fig. 5b**). We conclude that A3G target location is based on positionally uncorrelated nonlinear translocation on long ssDNA.

DNA tethering by monomeric A3G

Like other APOBEC proteins, A3G naturally forms homodimers and multimers[17,23,49–52], and binds ssDNA with high affinity (apparent K_d ~50–75 nM[39,49,53]). The fact that it is catalytically active as a monomer[54] and does not seem to bind DNA with cooperativity[49] suggests that the A3G monomer is sufficient to bind DNA. Moreover, mutations in either one of the two zinc-finger domains of A3G resulted in only approximately two-fold to four-fold higher K_d for a single-stranded deoxyoligonucleotide[53], demonstrating that either the N- or the C-terminal domains are sufficient to bind DNA independently. Intersegmental transfer by simultaneous binding of two DNA segments is therefore possible for dimeric or multimeric A3G, as well as for the monomeric protein itself.

To assess whether A3G binds two (or more) DNA fragments simultaneously, we performed electrophoretic mobility shift assays (EMSA). A3G binding to the 30–40-nt S_{35} or to the 80-nt S_{Eco} (**Fig. 6a**) or S_{NoC} (oligonucleotide not containing A3G target site, data not shown) was dose dependant. Whereas binding of S_{Eco} produced two to four shifted bands, binding to S_{35} produced one shifted band at similar concentrations, indicating that A3G bound DNA as a defined enzymatic species. Furthermore, band(I) of S_{35} migrated just below band(I) of S_{Eco}, implying that the first consists of A3G bound to two DNA fragments. Parallel DNA binding by A3G was further demonstrated by using S_{35} and S_{160} at E/S = 1:2, where A3G bound most of S_{35} but only ~50% of S_{160} (**Supplementary Fig. 4a** online). It is therefore likely that band(II) of S_{Eco}, which was observed at excess substrate (**Fig. 6a**), denotes A3G bound to two DNA fragments.

To identify the nature of this band, we compared the shifting of the 80-nt S_{Eco} to that of the 160-nt S_{160} (**Fig. 6b**). Band(I) of S_{Eco} migrated just below S_{160}, indicating that the band consisted of A3G bound to one DNA fragment. Notably, band(II) of S_{Eco} aligned with band(I) of S_{160}, indicating simultaneous binding of two 80-nt fragments by A3G. Early encounters between A3G and S_{160} assessed by 'real-time PAGE', showed that band(II) of S_{160} formed during the first 15 s of incubation (**Supplementary Fig. 4b**). To exclude the possibility that band(II) consists of two (or more) A3G species bound to one DNA molecule, we tested A3G binding at increasing S_{Eco} concentrations. At [S] ≫ [E], there is a low probability for more than one A3G molecule to bind a single DNA molecule; therefore, it could be expected that a band denoting more than a single A3G molecule bound to DNA would disappear. The formation of S_{Eco} band(II) was not affected at 5× to 40× molar excess of substrate (**Supplementary Fig. 4c**), consistent with a single A3G species bound to two DNA molecules. It could also be expected that excess enzyme conditions will disfavor binding of A3G to two 'free' DNA fragments. Indeed, at E/S = 2:1, the formation of band(II) as well as band(I) of S_{Eco} was reduced, in favor of higher-order enzyme-DNA complexes (**Supplementary Fig. 4d**). Preincubation of A3G with the unlabeled 40-nt ribooligonucleotide S_{JL}, followed by incubation with S_{Eco}, did not inhibit the formation of S_{Eco} band(I) nor band(II), indicating that RNA binding does not inhibit transfer of A3G to DNA (**Supplementary Fig. 4e**). Notably, an additional band between band(I) and (II) was visible, probably denoting a ternary A3G-DNA-RNA complex.

To define the enzymatic species bound to DNA, we used the 33-kDa bacteriophage T_4 ssDNA binding protein (SSB, gp32) which binds ssDNA as a monomer with cooperativity[55]. At excess enzyme, SSB binding produced three shifted DNA bands, two higher and one lower than band(I) of A3G (**Fig. 6c**). These bands probably represent cooperative binding of one, two and three SSB proteins, indicating that A3G bound DNA as a monomer. To determine whether monomeric A3G is the active enzyme form, we subjected purified A3G to size-exclusion chromatography using a fast protein liquid chromatography (FPLC) apparatus and calculated the relative specific activity of A3G in individual fractions. Most A3G (85–90%) resided in RNA-independent multimers, ranging from 4-mers to ~16-mers (**Fig. 6d**). Although different multimeric forms of A3G had similar specific activity, the dimeric and monomeric forms had three-fold and four-fold higher specific activity, respectively. These results suggest that, in the presence of ssDNA, A3G multimers dissociate to dimers in a slow equilibrium, and then to monomers in a rapid equilibrium.

DISCUSSION

Detection of A3G in HIV-$1^{vif(-)}$ but not in wild-type virions enabled correlating A3G activity to the loss of viral infectivity[25]. The number of A3G molecules incorporated into HIV-$1^{vif(-)}$ was previously estimated to be 7 (± 4), suggesting that virion incorporation of only a few molecules of A3G is sufficient to inhibit HIV-1 replication[56]. This is similar to our own estimative of 4–9 active A3G molecules per virion for *vif*$^{(-)}$ HIV-1. Using a highly sensitive assay for detection of cytidine deamination, we found that endogenous A3G expressed in H9 lymphoblastoid T cells is incorporated into wild-type HIV-1

virions (**Fig. 2**), and calculated an average of 0.3–0.8 active A3G molecules per virion. One A3G molecule might not be sufficient for virion inactivation, or, paradoxically, even have a net positive effect on viral infectivity, for example, by inducing mutations that promote drug resistance or immune evasion[57,58]. However, incorporation of several A3G molecules will probably render virions inactive, reducing the amplitude of viral infection (see below).

A3G acts in cytoplasmic reverse-transcription complexes, in concert with the formation of newly synthesized ssDNA. The A3G window of activity is therefore limited to the time interval during which the viral DNA remains single stranded[39]. Antiviral activity via detrimental hypermutation in limited time requires an efficient mechanism for enzyme-target location. We show that A3G is an extremely efficient enzyme that catalyzes cytidine deamination on an 80-nt oligonucleotide at an apparent rate of 2.0×10^8 M^{-1} s^{-1}, approaching the upper theoretical limit of simple diffusion control. However, antiviral efficacy in the context of retroviral reverse transcription requires more than an efficient enzyme (**Fig. 1**), particularly considering the low numbers of enzymatically active A3G molecules found associated to each virion, as discussed above. Dissociation of A3G from the viral RNA or DNA (as in the case of jumping) might result in permanent or long-term disengagement from the reverse-transcription complex. In contrast, translocation by tethering two DNA segments will greatly reduce the risk of enzyme disengagement by ensuring a 'foot on the ground' for A3G and that continuous contact with viral DNA is maintained. Furthermore, as polymerization and RNase H activities of HIV-1 (and other retroviruses) reverse transcriptases are functionally uncoupled, intermittent cleavage by RNase H leaves many RNA fragments annealed to the newly synthesized viral DNA[45,59,60]. Although not determined *in vivo*, the size of these RNA-DNA duplexes *in vitro* is >100-nt[59]. Enzyme progression by linear translocation (sliding) will therefore lead to frequent dissociations from DNA, or confine A3G to ssDNA islands; positionally correlated nonlinear translocation (microscopic jumping) will lead to nonproductive translocation in cases where docking occurs on a DNA-RNA duplex, a surface not readily bound by A3G. Only translocation by nonlinear intra- and intersegmental transfer would eliminate these physical barriers without risking enzyme disengagement.

To gain insights into A3G target location, we assessed the activity of single A3G molecules on adjacent cytidines and on separate target motifs within short and long ssDNA templates. In a previous report[49], Chelico *et al.* showed that A3G acts processively on single stranded deoxyoligonucleotides containing two or three separated target motifs. Measuring initial deamination rates on oligonucleotide substrates containing two or three separate target motifs under standard conditions have confirmed that A3G seems to act processively on separate targets (**Fig. 5a**). However, kinetic analyses of local activity on single polycytidine targets have shown distributive activity directing single cytidine deamination per DNA binding (**Fig. 4**), indicating that A3G cannot be considered as intrinsically processive. This was further demonstrated when intermolecular translocation abolished enzyme processivity at increased oligonucleotide concentrations while maintaining the same E/S ratio (**Fig. 5b**).

A fundamental difference between the present study and the previous one[49] concerns the mechanism of A3G-induced hypermutation. Facilitated diffusion of DNA binding proteins is suggested to occur in a positionally correlated fashion—by a linear sliding motion or microscopic jumping—or in a positionally uncorrelated fashion—by macroscopic jumping or intersegmental transfer. Whereas Chelico *et al.* suggested that A3G translocates in a positionally correlated fashion, that is, by sliding (80% of the time) and microscopic jumping (20%), we present several lines of evidence incompatible with such a mechanism. We show that A3G undergoes nonlinear, positionally uncorrelated translocation, and present data in favor of intersegmental transfer. Specifically, assessment of the cytidine-deamination kinetics using oligonucleotide substrates suggested that A3G undergoes nonlinear translocation (**Figs. 4** and **5**). We used *in vitro* rolling-circle amplification to synthesize long (5–10 kb) ssDNA substrates containing A3G target sites at 100-nt intervals and showed that A3G directed numerous positionally uncorrelated deamination events, leading to dispersed hypermutation of single DNA molecules (**Fig. 5c**). The A3G 'deamination trail' observed on short and long ssDNA, along with A3G's ability to bind two DNA segments simultaneously (**Fig. 6**) imply intersegmental transfer as a major path in A3G targeting.

A3G derived from HEK-293T cells resided mostly in RNA-independent multimers (**Fig. 6d**), implying that A3G associated with HMM ribonucleoprotein complexes formed in these cells is recruited as a multimeric protein. This is consistent with the structure of HMM complexes resembling symmetrical association of A3G dimers[51]. Whereas HMM-associated A3G is catalytically inactive[47] and is not incorporated into HIV-1 virions[44], it was reported that A3G multimers are recruited to the plasma membrane for packaging into HIV-1 (ref. 52), further corroborating our data. It was recently shown that, in the presence of salt (5 mM $MgCl_2$) and DNA, A3G purified from insect Sf9 cells exists mostly in oligomers and to a lesser extent in monomers[50]. However, our data clearly show that even in the presence of salt (7.5 mM $MgCl_2$), the active A3G form that binds DNA is monomeric (**Fig. 6**). Thus, we propose that multimeric cellular A3G incorporated into viruses or cytoplasmic reverse-transcription complexes dissociates to multiple functional monomeric units upon cDNA synthesis, each unit working individually toward DNA inactivation.

In conclusion, we show that A3G-induced hypermutation is mediated by intersegmental transfer. This mechanism, using two nucleic acid binding domains in A3G, might be essential for retroviral inactivation, as single-domain A3 proteins such as A3A and A3C show markedly reduced hypermutation and antiviral activity, albeit being highly active as cytidine deaminases and efficiently packaged into virions[61,62]. Considering the hallmark of HIV-1 replication and a putative quantitative effect of A3G in virions, it is not unlikely that viral strategies aimed at impeding A3G intersegmental transfer could not only prevent inactivation of the viral DNA, but might also contribute to viral fitness[57,58].

METHODS

Purification of A3G. We used the vector pcDNA3.1-A3G-myc-His_6[40] to express a C-terminally tagged A3G protein in human embryonic kidney (HEK) 293T cells. Cells ($\sim 5 \times 10^8$) were harvested 48 h after transfection, washed three times in PBS and suspended in lysis buffer (50 mM Tris, pH 8.0, 1 mM PMSF (Sigma), 10% (v/v) glycerol and 0.8% (v/v) NP-40), to a final concentration of 20,000 cells per microliter. Following incubation for 10 min on ice, cell debris and nuclei were pelleted by centrifugation at 10,000*g* for 20 min. The soluble fraction was adjusted to 0.8 M NaCl and treated with 50 μg ml^{-1} RNase A (Sigma) for 15 min at 37 °C and 1 h at 25 °C. Treated lysates were then added to 50 μl of nickel–nitrilotriacetic acid (Ni-NTA) agarose (Qiagen), mixed on an end-over-end shaker for 1 h at 4 °C and loaded onto a standard chromatography column (Biorad). Following extensive washing with wash buffer (50 mM Tris, pH 8.0, 0.3 M NaCl, 10% (v/v) glycerol) containing 30–50 mM imidazole, bound proteins were eluted four times in wash buffer containing 120 mM imidazole. Protein samples were resolved by SDS-PAGE and stained with Imperial protein stain (Pierce) or transferred to polyvinylidene difluoride (PVDF) membranes (Pall) and subjected to western blotting with anti-myc monoclonal antibody (Santa-Cruz). We assessed A3G

concentration and purity by densitometry scanning of stained gels (**Fig. 3a**), comparing band intensity to that of a predetermined protein marker, and by a Bradford assay.

Deamination assay. A3G deamination reactions were performed in a total volume of 10 µl in 25 mM Tris, pH 7.0, and 1–1,000 fmol single-stranded deoxyoligonucleotide substrate (Integrated DNA Technologies) at 37 °C (standard conditions). Kinetic assays were performed at [E] ≪ [S] so that the overall product formation fell below 10% (5% in K_m assays) of the substrate. The reaction was terminated by heating to 95 °C for 5 min. One fmol of the reaction mixture was used for PCR amplification performed in 20 µl buffer Y (Larova), using the following program: 1 cycle at 95 °C for 3 min, followed by 15 cycles of annealing at 61 °C for 30 s and denaturing at 94 °C for 30 s. Aliquots of the PCR products (10 µl) were incubated with the relevant restriction enzyme (NEB, Fermentas) (**Supplementary Table 1**) for 1 h at 37 °C. Completion of the restriction reaction was verified by using positive-control substrates containing CCU instead of CCC (**Supplementary Fig. 1b**). Restriction-reaction products were loaded onto 14% gels and separated by PAGE. Gels were stained with SYBR gold nucleic acid stain (Molecular Probes) diluted 1:10,000 in 0.5× Tris-Borate-EDTA buffer (TBE, pH 7.8), visualized by UV light (312 nm), captured by an Olympus C-5050 charge-coupled device (CCD) camera and analyzed by optical density (OD) scan using the TINA2.0 densitometry software (Raytest). Mixtures of known amounts of CCC and CCU substrates, simulating increasing deamination levels, were used to determine PCR and SYBR-gold staining linearity (**Supplementary Fig. 1a**).

Assessment of deaminase activity in virions. Wild-type or *vif*$^{(-)}$ HIV-1_{HXBII} were produced in 293T cells, harvested from culture medium 48 h after transfection and used to infect 10^7 human T lymphoblastoid H9 or SupT1 cells. Culture medium was harvested 5 d after infection, centrifuged to pellet cells, clarified through a 0.22 µm filter, and centrifuged for 1.5 h at 100,000*g* through a 20% sucrose cushion. Pelleted virus was suspended in lysis buffer containing 25 mM Tris, pH 7.0 and 0.1% (v/v) Triton X-100, and used for deamination assays, assessment of the p24 antigen content using HIV-1 p24 Antigen Capture Assay kit (AIDS Vaccine Program, NCI, Frederick), or detection of A3G by Western analysis using anti-A3G (C-terminal) antiserum (provided by J. Lingappa, Department of Pathobiology, University of Washington). For deamination assays, viruses (0.6–18 ng p24) were incubated with S_{Eco} (10 fmol) in buffer containing 25 mM Tris, pH 7.0, and 0.1% (v/v) Triton X-100, with or without 50 µg ml^{-1} RNase A (Sigma), for 1 h at 37 °C. For calculating A3G content in virions, we determined the amount of A3G per 1 ng p24 by comparing the virion-associated deaminase activity to the activity of predetermined amounts of purified A3G. We calculated A3G content in the wild-type virus as follows (**Fig. 2**):

Activity of virion A3G versus 1.75 pg purified A3G = 1.63/1.65 = 0.987.
Amount of virion A3G = 0.987 × 1.75 pg = 1.72 pg.
A3G:p24 weight ratio = 1.72 pg:6300 pg = 1:3,663.
A3G:p24 molar ratio = 1:6,520.

Assuming approximately 2,000 or 5,000 p24 molecules per virion[45,46], we calculated an average of 0.3–0.8 A3G molecules per virion. Similar calculations were performed in the case of the *vif*$^{(-)}$ virus.

Determination of A3G segmental transfer on long ssDNA. We generated ssDNA templates by rolling-circle amplification as follows: Circular DNA (Circ; 50 pmol) was incubated with 1 U T_4 polynucleotide kinase (Fermentas) in T_4 ligase buffer (New England Biolabs) in 20 µl reaction volume, for 30 min at 37 °C. Following heat inactivation, phosphorylated Circ was annealed to pCirc (100 pmol) and incubated with 1 U T_4 ligase (NEB) for 13 h at 16 °C. Following heat inactivation, ligated Circ (0.5–1 pmol) was elongated with 15 U klenow fragment (exo$^-$) of *E. coli* (NEB), in NEBuffer 1 (NEB) supplemented with 2 mM dNTPs (Larova), for 3 h at 37 °C. Rolling-circle amplification products containing a CCC target in 100-nt intervals were approximately 5–10 kb long, as determined by denaturing PAGE and atomic force microscopy (data not shown). A3G deamination was performed in rolling-circle amplification tubes adjusted to 0.5 nM A3G (E/S = 1:50–100), 20 mM Tris, pH 7.0, and 0.1 mg ml^{-1} BSA, for 8 min at 37 °C. Reactions were terminated by phenol extraction followed by ethanol precipitation of DNA. Cleavage of deaminated ssDNA was performed by incubation with 1 U uracil DNA glycosylase (UDG, NEB) for 30 min at 37 °C, followed by adjusting reactions to 150 mM NaOH and further incubating for 30 min at 37 °C. Reactions were then neutralized with HCl and DNA was ethanol precipitated. DNA was suspended in 50% (v/v) formamide, incubated for 10 min at 65 °C and separated by 5% Urea-PAGE. Following staining with SYBR gold, gels were visualized by UV light and captured with a CCD. Total deamination was determined by the substrate usage and assays were performed so that less than 15% of the substrate (75–150 fmol) was deaminated. Assuming 50–100 CCC targets per DNA, nonprocessive random deamination would result in 50–100 differently sized products of 1–3 fmol each. Considering the lower sensitivity threshold (50 fmol of the 200-nt fragment, 10 fmol of the 1,000-nt fragment) of the assay, this activity would produce undetectable amounts of product DNA. The DNA bands visualized in gels under these conditions (**Fig. 5c**) must therefore represent A3G segmental transfer within DNA molecules required to produce an approximately 5-fold to 25-fold increase in the molarity of the detected DNA fragments.

Gel filtration. A3G containing samples were resolved on a Superdex 200 300/10 GL column (GE Healthcare) using an Akta basic FPLC apparatus, at a flow rate of 0.5 ml min^{-1}. The column was equilibrated with 10 mM Tris, pH 7.0, and 0.3 ml or 0.5 ml samples were collected. Samples were stored at –20 °C for use in deamination assays, or concentrated in a lyophilizer × 30 and used for western blotting. Gel-filtration low- and high-molecular-weight calibration kits (GE Healthcare) were used for molecular-weight determination.

Electrophoretic mobility shift assay. Deoxyoligonucleotides (10 pmol) were 3′ labeled with dATP-biotin using 10 U terminal deoxynucleotidyl transferase (NEB) in NEBuffer 4 supplemented with 0.25 mM $CoCl_2$ and 10 µM dATP-biotin (Invitrogen). Labeled oligonucleotides (50–800 fmol) were incubated with A3G at the indicated E/S ratios, for 8 min at 37 °C, in EMSA buffer: 50 mM Tris, pH 7.0, 50 mM NaCl, 7.5 mM $MgCl_2$, 0.1 mg ml^{-1} BSA and 10% (v/v) glycerol, in 10 µl reaction volume. Samples were resolved by 4% or 6% native PAGE, transferred to a Hybond N nylon membrane (GE Healthcare) using a semidry transfer apparatus (Biorad), and UV cross-linked at 312 nm for 15 min. Following blocking with 5% skim milk, the membrane was treated with horseradish peroxidase–conjugated sterptavidine (Jackson) for 20 min at room temperature, washed four times with TBS (pH 7.4) and visualized by enhanced chemiluminescence.

Note: Supplementary information is available on the Nature Structural & Molecular Biology website.

ACKNOWLEDGMENTS

This work was carried out in the Krueger Laboratory with the support of N. and L. Glick, and P. and M. Weiss. We thank K. Strebel (US National Institutes of Health (NIH), Bethesda, Maryland, USA) for providing pcDNA-APOBEC3G. We thank E. Pikarsky, R. Harris and H. Matsuo for constructive and helpful discussion, and S. Amir for editing this manuscript. Anti-APOBEC3G-C-terminal antibody was obtained from J. Lingappa through the NIH AIDS Research and Reference Reagent Program, Division of AIDS, NIAID, NIH. This work was supported in part by the Israel Ministry of Industry Trade & Labor via the Nofar program, the Israel Ministry of Health and the United States-Israel Binational Science Foundation (BSF).

AUTHOR CONTRIBUTIONS

R.N. and M.K. designed the experiments and wrote the paper; R.N. performed the experiments; E.B.-R. and T.S. contributed reagents and provided assistance.

Published online at http://www.nature.com/nsmb/
Reprints and permissions information is available online at http://npg.nature.com/reprintsandpermissions/

1. Riggs, A.D., Bourgeois, S. & Cohn, M. The *lac* repressor-operator interaction. 3. Kinetic studies. *J. Mol. Biol.* **53**, 401–417 (1970).
2. Berg, O.G., Winter, R.B. & von Hippel, P.H. Diffusion-driven mechanisms of protein translocation on nucleic acids. 1. Models and theory. *Biochemistry* **20**, 6929–6948 (1981).
3. Winter, R.B., Berg, O.G. & von Hippel, P.H. Diffusion-driven mechanisms of protein translocation on nucleic acids. 3. The *Escherichia coli lac* repressor–operator interaction: kinetic measurements and conclusions. *Biochemistry* **20**, 6961–6977 (1981).

4. von Hippel, P.H. & Berg, O.G. Facilitated target location in biological systems. *J. Biol. Chem.* **264**, 675–678 (1989).
5. von Hippel, P.H. Protein-DNA recognition: new perspectives and underlying themes. *Science* **263**, 769–770 (1994).
6. Stanford, N.P., Szczelkun, M.D., Marko, J.F. & Halford, S.E. One- and three-dimensional pathways for proteins to reach specific DNA sites. *EMBO J.* **19**, 6546–6557 (2000).
7. Houtsmuller, A.B. *et al.* Action of DNA repair endonuclease ERCC1/XPF in living cells. *Science* **284**, 958–961 (1999).
8. Lever, M.A., Th'ng, J.P., Sun, X. & Hendzel, M.J. Rapid exchange of histone H1.1 on chromatin in living human cells. *Nature* **408**, 873–876 (2000).
9. Misteli, T. Protein dynamics: implications for nuclear architecture and gene expression. *Science* **291**, 843–847 (2001).
10. Gorman, J. & Greene, E.C. Visualizing one-dimensional diffusion of proteins along DNA. *Nat. Struct. Mol. Biol.* **15**, 768–774 (2008).
11. Menetski, J.P. & Kowalczykowski, S.C. Transfer of recA protein from one polynucleotide to another. Kinetic evidence for a ternary intermediate during the transfer reaction. *J. Biol. Chem.* **262**, 2085–2092 (1987).
12. Kozlov, A.G. & Lohman, T.M. Kinetic mechanism of direct transfer of *Escherichia coli* SSB tetramers between single-stranded DNA molecules. *Biochemistry* **41**, 11611–11627 (2002).
13. Deibert, M., Grazulis, S., Sasnauskas, G., Siksnys, V. & Huber, R. Structure of the tetrameric restriction endonuclease NgoMIV in complex with cleaved DNA. *Nat. Struct. Biol.* **7**, 792–799 (2000).
14. Halford, S.E., Gowers, D.M. & Sessions, R.B. Two are better than one. *Nat. Struct. Biol.* **7**, 705–707 (2000).
15. Lewis, M. *et al.* Crystal structure of the lactose operon repressor and its complexes with DNA and inducer. *Science* **271**, 1247–1254 (1996).
16. Guo, F., Gopaul, D.N. & van Duyne, G.D. Structure of Cre recombinase complexed with DNA in a site-specific recombination synapse. *Nature* **389**, 40–46 (1997).
17. Jarmuz, A. *et al.* An anthropoid-specific locus of orphan C to U RNA-editing enzymes on chromosome 22. *Genomics* **79**, 285–296 (2002).
18. Harris, R.S. & Liddament, M.T. Retroviral restriction by APOBEC proteins. *Nat. Rev. Immunol.* **4**, 868–877 (2004).
19. Izumi, T., Shirakawa, K. & Takaori-Kondo, A. Cytidine deaminases as a weapon against retroviruses and a new target for antiviral therapy. *Mini Rev. Med. Chem.* **8**, 231–238 (2008).
20. Vartanian, J.P., Guetard, D., Henry, M. & Wain-Hobson, S. Evidence for editing of human papillomavirus DNA by APOBEC3 in benign and precancerous lesions. *Science* **320**, 230–233 (2008).
21. Bhattacharya, S., Navaratnam, N., Morrison, J.R., Scott, J. & Taylor, W.R. Cytosine nucleoside/nucleotide deaminases and apolipoprotein B mRNA editing. *Trends Biochem. Sci.* **19**, 105–106 (1994).
22. Reizer, J., Buskirk, S., Bairoch, A., Reizer, A. & Saier, M.H., Jr. A novel zinc-binding motif found in two ubiquitous deaminase families. *Protein Sci.* **3**, 853–856 (1994).
23. Navarro, F. *et al.* Complementary function of the two catalytic domains of APOBEC3G. *Virology* **333**, 374–386 (2005).
24. Hache, G., Liddament, M.T. & Harris, R.S. The retroviral hypermutation specificity of APOBEC3F and APOBEC3G is governed by the C-terminal DNA cytosine deaminase domain. *J. Biol. Chem.* **280**, 10920–10924 (2005).
25. Sheehy, A.M., Gaddis, N.C., Choi, J.D. & Malim, M.H. Isolation of a human gene that inhibits HIV-1 infection and is suppressed by the viral Vif protein. *Nature* **418**, 646–650 (2002).
26. Harris, R.S. *et al.* DNA deamination mediates innate immunity to retroviral infection. *Cell* **113**, 803–809 (2003).
27. Lecossier, D., Bouchonnet, F., Clavel, F. & Hance, A.J. Hypermutation of HIV-1 DNA in the absence of the Vif protein. *Science* **300**, 1112 (2003).
28. Mangeat, B. *et al.* Broad antiretroviral defence by human APOBEC3G through lethal editing of nascent reverse transcripts. *Nature* **424**, 99–103 (2003).
29. Marin, M., Rose, K.M., Kozak, S.L. & Kabat, D. HIV-1 Vif protein binds the editing enzyme APOBEC3G and induces its degradation. *Nat. Med.* **9**, 1398–1403 (2003).
30. Zhang, H. *et al.* The cytidine deaminase CEM15 induces hypermutation in newly synthesized HIV-1 DNA. *Nature* **424**, 94–98 (2003).
31. Rosler, C., Kock, J., Malim, M.H., Blum, H.E. & von Weizsacker, F. Comment on "Inhibition of hepatitis B virus replication by APOBEC3G". *Science* **305**, 1403 author reply 1403 (2004).
32. Turelli, P., Mangeat, B., Jost, S., Vianin, S. & Trono, D. Inhibition of hepatitis B virus replication by APOBEC3G. *Science* **303**, 1829 (2004).
33. Suspene, R. *et al.* Extensive editing of both hepatitis B virus DNA strands by APOBEC3 cytidine deaminases *in vitro* and *in vivo*. *Proc. Natl. Acad. Sci. USA* **102**, 8321–8326 (2005).
34. Kock, J. & Blum, H.E. Hypermutation of hepatitis B virus genomes by APOBEC3G, APOBEC3C and APOBEC3H. *J. Gen. Virol.* **89**, 1184–1191 (2008).
35. Esnault, C. *et al.* APOBEC3G cytidine deaminase inhibits retrotransposition of endogenous retroviruses. *Nature* **433**, 430–433 (2005).
36. Schumacher, A.J., Nissley, D.V. & Harris, R.S. APOBEC3G hypermutates genomic DNA and inhibits Ty1 retrotransposition in yeast. *Proc. Natl. Acad. Sci. USA* **102**, 9854–9859 (2005).
37. Dutko, J.A., Schafer, A., Kenny, A.E., Cullen, B.R. & Curcio, M.J. Inhibition of a yeast LTR retrotransposon by human APOBEC3 cytidine deaminases. *Curr. Biol.* **15**, 661–666 (2005).
38. Chiu, Y.L. *et al.* High-molecular-mass APOBEC3G complexes restrict Alu retrotransposition. *Proc. Natl. Acad. Sci. USA* **103**, 15588–15593 (2006).
39. Yu, Q. *et al.* Single-strand specificity of APOBEC3G accounts for minus-strand deamination of the HIV genome. *Nat. Struct. Mol. Biol.* **11**, 435–442 (2004).
40. Kao, S. *et al.* The human immunodeficiency virus type 1 Vif protein reduces intracellular expression and inhibits packaging of APOBEC3G (CEM15), a cellular inhibitor of virus infectivity. *J. Virol.* **77**, 11398–11407 (2003).
41. Stopak, K., de Noronha, C., Yonemoto, W. & Greene, W.C. HIV-1 Vif blocks the antiviral activity of APOBEC3G by impairing both its translation and intracellular stability. *Mol. Cell* **12**, 591–601 (2003).
42. Yu, X. *et al.* Induction of APOBEC3G ubiquitination and degradation by an HIV-1 Vif-Cul5-SCF complex. *Science* **302**, 1056–1060 (2003).
43. Opi, S. *et al.* Human immunodeficiency virus type 1 Vif inhibits packaging and antiviral activity of a degradation-resistant APOBEC3G variant. *J. Virol.* **81**, 8236–8246 (2007).
44. Soros, V.B., Yonemoto, W. & Greene, W.C. Newly synthesized APOBEC3G is incorporated into HIV virions, inhibited by HIV RNA, and subsequently activated by RNase H. *PLoS Pathog.* **3**, e15 (2007).
45. John, M., Coffin, S.H.H. & Varmus, H.E. *Retroviruses* (Cold Spring Harbor Laboratory Press, Cold Spring Harbor, NY, 1999).
46. Briggs, J.A. *et al.* The stoichiometry of Gag protein in HIV-1. *Nat. Struct. Mol. Biol.* **11**, 672–675 (2004).
47. Chiu, Y.L. *et al.* Cellular APOBEC3G restricts HIV-1 infection in resting CD4+ T cells. *Nature* **435**, 108–114 (2005).
48. Fersht, A. *Enzyme Structure and Mechanism* (Freeman, New York, NY, 1985).
49. Chelico, L., Pham, P., Calabrese, P. & Goodman, M.F. APOBEC3G DNA deaminase acts processively 3′ → 5′ on single-stranded DNA. *Nat. Struct. Mol. Biol.* **13**, 392–399 (2006).
50. Chelico, L., Sacho, E.J., Erie, D.A. & Goodman, M.F. A model for oligomeric regulation of APOBEC3G cytosine deaminase-dependent restriction of HIV. *J. Biol. Chem.* **283**, 13780–13791 (2008).
51. Wedekind, J.E. *et al.* Nanostructures of APOBEC3G support a hierarchical assembly model of high molecular mass ribonucleoprotein particles from dimeric subunits. *J. Biol. Chem.* **281**, 38122–38126 (2006).
52. Burnett, A. & Spearman, P. APOBEC3G multimers are recruited to the plasma membrane for packaging into human immunodeficiency virus type 1 virus-like particles in an RNA-dependent process requiring the NC basic linker. *J. Virol.* **81**, 5000–5013 (2007).
53. Iwatani, Y., Takeuchi, H., Strebel, K. & Levin, J.G. Biochemical activities of highly purified, catalytically active human APOBEC3G: correlation with antiviral effect. *J. Virol.* **80**, 5992–6002 (2006).
54. Opi, S. *et al.* Monomeric APOBEC3G is catalytically active and has antiviral activity. *J. Virol.* **80**, 4673–4682 (2006).
55. Bittner, M., Burke, R.L. & Alberts, B.M. Purification of the T4 gene 32 protein free from detectable deoxyribonuclease activities. *J. Biol. Chem.* **254**, 9565–9572 (1979).
56. Xu, H. *et al.* Stoichiometry of the antiviral protein APOBEC3G in HIV-1 virions. *Virology* **360**, 247–256 (2007).
57. Mulder, L.C., Harari, A. & Simon, V. Cytidine deamination induced HIV-1 drug resistance. *Proc. Natl. Acad. Sci. USA* **105**, 5501–5506 (2008).
58. Pillai, S.K., Wong, J.K. & Barbour, J.D. Turning up the volume on mutational pressure: is more of a good thing always better? (a case study of HIV-1 Vif and APOBEC3). *Retrovirology* **5**, 26 (2008).
59. DeStefano, J.J. *et al.* Polymerization and RNase H activities of the reverse transcriptases from avian myeloblastosis, human immunodeficiency, and Moloney murine leukemia viruses are functionally uncoupled. *J. Biol. Chem.* **266**, 7423–7431 (1991).
60. Wisniewski, M., Balakrishnan, M., Palaniappan, C., Fay, P.J. & Bambara, R.A. Unique progressive cleavage mechanism of HIV reverse transcriptase RNase H. *Proc. Natl. Acad. Sci. USA* **97**, 11978–11983 (2000).
61. Langlois, M.A., Beale, R.C., Conticello, S.G. & Neuberger, M.S. Mutational comparison of the single-domained APOBEC3C and double-domained APOBEC3F/G anti-retroviral cytidine deaminases provides insight into their DNA target site specificities. *Nucleic Acids Res.* **33**, 1913–1923 (2005).
62. Gooch, B.D. & Cullen, B.R. Functional domain organization of human APOBEC3G. *Virology* **379**, 118–124 (2008).